Development of A Dynamic Quadruped with Tunable, Compliant Legs

Fuchen Chen¹, Weijia Tao¹, and Daniel M. Aukes¹

Abstract—To facilitate the study of how passive leg stiffness influences locomotion dynamics and performance, we have developed an affordable and accessible 400 g quadruped robot driven by tunable compliant laminate legs, whose series and parallel stiffness can be easily adjusted; fabrication only takes 2.5 hours for all four legs. The robot can trot at 0.52 m/s or 4.4 body lengths per second with a 3.2 cost of transport (COT). Through locomotion experiments in both the real world and simulation we demonstrate that legs with different stiffness have an obvious impact on the robot's average speed, COT, and pronking height. When the robot is trotting at 4 Hz in the real world, changing the leg stiffness yields a maximum improvement of 37.1% in speed and 62.0% in COT, showing its great potential for future research on locomotion controller designs and leg stiffness optimizations.

I. INTRODUCTION

This paper presents a preliminary attempt to develop affordable and accessible quadrupeds to facilitate the study of how passive leg stiffness influences locomotion dynamics and performance. As shown in Fig. ??, our proposed robot is composed of four 15 g, finger-length legs. These compliant, laminated fiberglass-composite mechanisms are designed and fabricated to facilitate tuning the passive parallel and series compliance. The complete robot has a footprint similar to an adult hand, weighs less than 400 grams, and is actuated by 8 servo motors. We aim to show that tuning the robot's passive leg stiffness is not only straightforward and low-cost, but also impactful on the performance of its locomotion for gaits like pronking and trotting. We believe this demonstrates the robot's potential for tuning and optimizing leg stiffness for niche and specialized applications. A secondary aim is to demonstrate its agreement with a simulated environment, which will be useful for future design optimization and control algorithm development.

We believe passive leg stiffness is one of the keys for tuning and optimizing quadrupedal locomotion capabilities. Through a variety of legged robots including but not limited to quadrupeds, researchers have demonstrated that properly tuned leg stiffness can improve stability [?], [?], impact resistance [?], efficiency [?], [?], peak power output [?], and payload capacity [?]. Physical springs have superior energy storage efficiency and actuation bandwidth compared to electric motors mimicking compliance via control [?]. They can also cut down system costs by alleviating power requirements and electro-mechanical complexity.

Despite its numerous advantages, passive leg stiffness is not present in several notable quadruped robots [?], [?], [?],



Fig. 1. Picture of the quadruped robot with tunable compliant laminate legs.

[?], [?]; this may be because integrating passive springs adds complexity to design, tuning, and control steps. Although many quadrupeds [?], [?], [?], demonstrate passive compliant legs and its associated performance, less research has focused on tuning passive leg stiffness for desired goals; this demands unique design features that are not typically included. To address the gaps that we see in the existing literature, we have focused on techniques to simplify and streamline the process of integrating compliance into the legs. We have carefully selected the position of actuators, transmissions, and supporting structures, in order to make legs and springs easily interchangeable. Affordability and fabrication time have remained a priority, because these aspects increase accessibility of legged robots to researchers inside and outside the field of robotics, as well as promote more rapid experimentation with real devices.

We propose that compliant, laminate legs designed and fabricated with origami-inspired approaches [?] can help address the above goals. The legs shown in Fig. ?? are fabricated as multi-layer, multi-material laminates that are cut, folded, and locked into three-dimensional mechanisms in order to provide both the desired kinematic motion and structural compliance. In this way, the tuning of the integrated system stiffness is accomplished by adjusting the length, width, and thickness of key regions of the laminate system instead of relying on commercially available springs. This approach makes it possible to pack complex mechanisms within tight weight and size constraints. The fabrication time, material cost, and assembly difficulty is also significantly

¹Ira A. Fulton Schools of Engineering, Arizona State University, Mesa, Arizona, 85212, USA. Email: {fchen65, wtao11, danaukes}@asu.edu

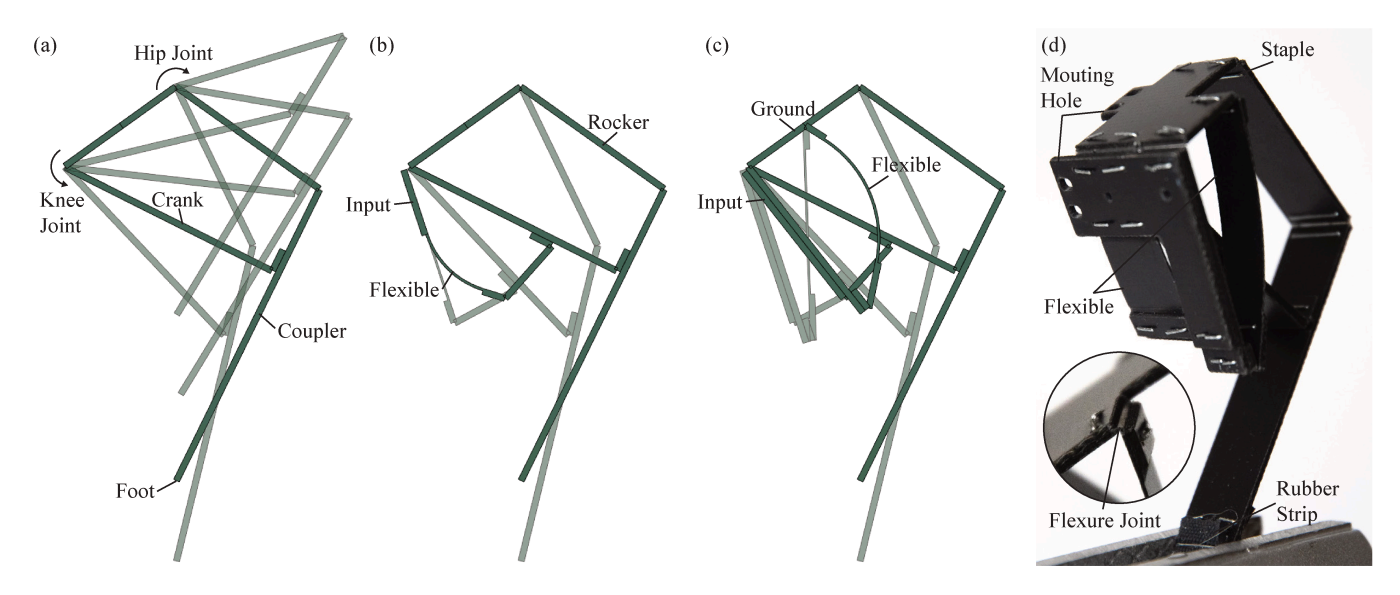


Fig. 2. (a) Motion of the four-bar linkage of the leg. (b) Deformation of the series spring of the leg (the parallel spring is hidden for clarity). (c) Deformation of the parallel spring of the leg. (d) Picture of the leg.

reduced in contrast with more conventional 3D printing, CNC machining, or other methods that utilize discrete parts – it takes 2.5 hours to make all four legs of our robot.

The contributions of the paper are: 1) a novel quadruped robot designed for tunable, passive leg stiffness and 2) demonstrations of how tuning leg stiffness can impact the performance of quadrupedal locomotion in both real-world and simulated experiments. The paper is laid out as follows: First, the design of the robot including the laminate legs and actuation modules is explained in section ??. The gait generation and simulation environment for the robot are then introduced in section ?? and section ?? In section ?? and section ??, we next show the measured stiffness profiles of three variants of our proposed leg design; their impact on our robot's locomotion is also unveiled with both experiments and simulation. We then conclude in section ?? with our thoughts on the future improvements and potential of this robot.

II. ROBOT DESIGN

As shown in Fig. ??, the entire robot consists of four actuation modules of identical design, sandwiched by two fiberglass sheets, the top of which houses the microcontroller, sensor, and battery. Laminate legs are fabricated separately and attached to the modules.

A. Leg

The proposed leg design is composed of three main components: a four-bar linkage responsible for extension and retraction, a laminate spring for providing series compliance, and a second spring for providing parallel compliance. The leg design and fabrication process is similar to those in our previous study [?] on single laminate leg jumping with nonlinear stiffness; we have added parallel compliance and made small adjustments to the overall design.

- 1) Four-bar Linkage: The main purpose of the four-bar linkage is to convert rotation into translation; its shape is optimized so that the foot fixed to its coupler link follows an approximated straight line when the crank is rotated, as illustrated in Fig. ?? (a). This design converts 1.16 rad rotation of the crank to a 6 cm change in effective leg length (distance between the hip joint and foot).
- 2) Laminate Springs: As revealed by our previous study, it is possible to fabricate torsion springs using folded laminate structures that result in a variety of stiffness profiles. Our laminate spring design is composed of two rigid links and one compliant link, all connected by flexure joints. Since one of the links is more flexible, the extra degree of freedom gained from that link's bending provides a restoring force under a torsional load, as illustrated in Fig. ?? (b) and (c). The stiffness coefficient of the spring may then be related to the geometry of the flexible link.

As illustrated in Fig. ?? (b), the leg's series compliance is determined by a laminate spring attached to the crank of the four-bar linkage, whose input connects to the knee servo. In this way, if a force is exerted on the foot, the spring deforms before transmitting forces to the input link and vice versa to absorb external impacts. As illustrated in Fig. ?? (c), a second laminate spring is attached between the input and the ground links to provide parallel compliance. During retraction, the knee servo stores energy in this second spring that can be then released during extension to modulate power delivery from the servos. Although both springs exhibit compliance in one direction due to their joint limits, the range provided is sufficient for the purposes of our study.

3) Fabrication: The leg consists of five layers: a 0.72 mm fiberglass¹ layer for structural rigidity, a 0.015 mm heat-

¹ACP Composites G-10/FR4

activated adhesive² layer, a 0.18 mm polyester sheet³ layer for flexure joints, another layer of the same adhesive, and a 0.45 mm fiberglass layer exposed selectively to soften the link. The leg is designed in Autodesk Fusion 360 in its flattened state, but can be folded up as an assembly and attached to other components. Python scripts are used to convert the design into cut patterns. After all material layer patterns are laser-cut, they are stacked and laminated with a heat press machine. A final cut releases the device from the surrounding scrap. The leg is then folded and locked into place with common office staples; these are also added around joints to prevent delamination. A rubber strip⁴ is attached to the foot to increase friction.

B. Actuation Module

Two servo motors⁵ with identical form factors but different gear ratios are selected to actuate each leg as shown in Fig. ??. These servos are light-weight and compact at 18 grams each, feature-rich with various sensory feedback and customizable controllers, affordable, and easy to use. The higher-gear-ratio variant is used for the knee joint, since it needs to support most of the robot's weight. The other motor swings the leg about the hip joint. Instead of actuating a leg in parallel [?], [?], [?], we chose to decouple each leg's motion because it reduces the power loss due to geometric work [?], enables usage of different actuators, and allows independent passive stiffness along those axes. Leg abduction and adduction motions are omitted because we initially plan to study the impact of passive stiffness in only the sagittal plane.

A cable-driven mechanism similar to the design by Buerger [?] and Hutter [?] is employed to transmit the knee servo rotation to the knee joint, as illustrated in Fig. ??. Different from other existing designs, the two pulleys are separated from each other and the cables go through a tiny slot formed by two thin pins located at the hip joint to prevent coupling between hip and knee angles. Despite the added assembly complexity and friction loss, this design removes the reflected weight of the knee servo from the hip servo transmission, keeping the total leg inertia minimal. It also allows mounting the two servos next to each other to keep the robot's footprint and body inertia small. Mounting holes are added to the servo arm and output pulley so that each leg can be attached to the module using four screws. Most parts of the housing are 3D printed except the bearings, cables, and mounting screws.

III. LOCOMOTION

Since the robot has two passive degrees of freedom from the springs and no sensory feedback, an open-loop Central Pattern Generator (CPG) has been initially selected for generating locomotory signals. CPGs are a group of coupled

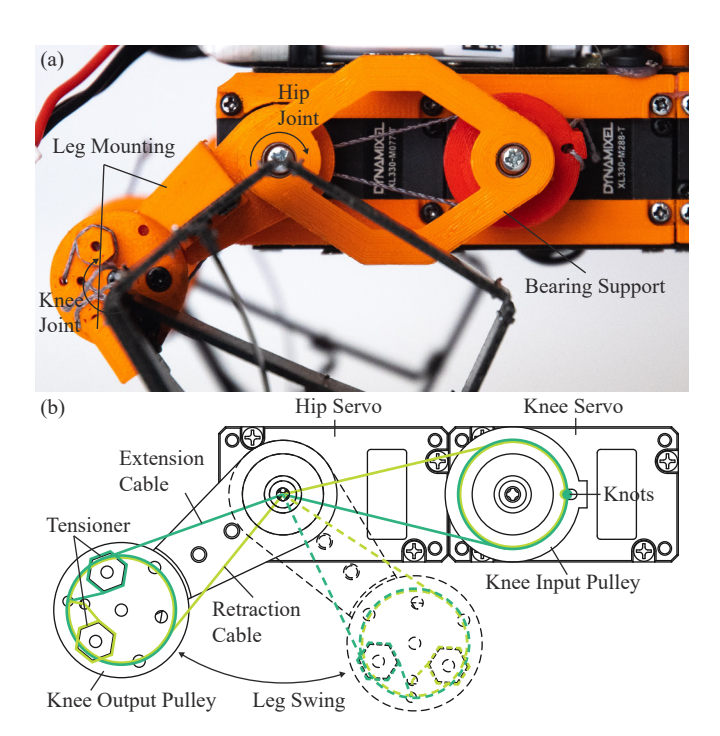


Fig. 3. (a) Picture of the actuation module. (b) Routing and components of the cable driven mechanism. The dashed lines show how the routing and knee angle is not affected when the hip rotates.

oscillators that generate rhythmic joint trajectories from nonrhythmic inputs [?]; they are capable of generating a variety of gait patterns for locomotion that are independent of system dynamics.

Our implementation of the CPG is similar to the ones used by Badri-Spröwitz [?], [?]; it contains four coupled oscillators described by the following differential equation:

$$\dot{\phi}_i = 2\pi f + \sum_{j=1}^4 \alpha_{\phi} c_{ij} sin(\phi_j - \phi_i - \psi_{ij}),$$
 (1)

where f is the gait frequency, $\alpha_{\phi}=1$ is a constant controlling the convergence rate, and i or j from 1 to 4 represents the oscillator related to the front left (FL), front right (FR), rear left (RL), and rear right (RR) leg respectively. c_{ij} is a element from the matrix c describing the coupling strength between oscillators and $c_{ij}=\begin{cases} 0, & i=j\\ 1, & i\neq j \end{cases}$ which is an element from the matrix ϕ describing the desired phase difference between oscillators and the values for the pronking and trotting gait used in the experiments are

$$\psi_{pronk} = \mathbf{0}, \psi_{trot} = \begin{bmatrix} 0 & -\pi & -\pi & 0 \\ \pi & 0 & 0 & \pi \\ \pi & 0 & 0 & \pi \\ 0 & -\pi & -\pi & 0 \end{bmatrix}.$$

The phase of each oscillator, wrapped into $[0, 2\pi)$, is then

²Drytac MHA

³Grafix Clear Dura-Lar

⁴McMaster-Carr 3846N38

⁵Robotis DYNAMIXEL xl330-m077-t and xl330-m288-t



Fig. 4. The robot pronking with S1 legs at 3Hz in the (a) real world and (b) simulation and the robot trotting with S1 legs at 4Hz in the (c) real world and (d) simulation.

converted to its respective hip joint angle with

$$\theta_i^h = a_i^h \cos(\phi_i^h) + o_i^h \,, \tag{2}$$

$$\theta_i^h = a_i^h cos(\phi_i^h) + o_i^h, \qquad (2)$$

$$\phi_i^h = \begin{cases} \frac{\phi_i}{2d}, & \phi_i < 2\pi d\\ \frac{\phi_i - 2\pi d}{2(1 - d)} + \pi, & \text{otherwise} \end{cases}, \qquad (3)$$

where d indicates the duty factor or percentage of the stance duration over one cycle, a_i^h is the hip swing amplitude, and o_i^h is the hip swing offset. The knee angle is also calculated from the oscillator's phase with

$$\theta_i^k = a_i^k \phi_i^k + o_i^k \,, \tag{4}$$

$$\phi_i^k = \begin{cases} 1, & 2\pi(d + o_r(1 - d)) < \phi_i < 2\pi \\ 0, & \text{otherwise} \end{cases} , \tag{5}$$

where \boldsymbol{a}_{i}^{k} is the knee retraction amplitude, \boldsymbol{o}_{i}^{k} is the knee retraction offset, and o_r is the knee retraction timing offset in percentage of the flight duration. Although the input knee angle behaves like a step function, the actual knee angle will be smoothed by the spring and motor dynamics. In our formulation, the hip angle is positive when swinging forward and the knee angle is positive when retracting.

A first-order differential equation is used to relate the desired CPG parameter value p_d with the actual value $p := [f, d, o_r, \bar{a}_i^h, a_i^k, o_i^h, o_i^k]$ for smooth transition between different gaits as in

$$\dot{p} = \alpha_p (p_d - p) \,, \tag{6}$$

where $\alpha_p = 10$ to keep the settling time within a second.

The CPG is implemented and runs at 100 Hz on the microcontroller and its output values are fed into the servos running their default PID angle control.

IV. SIMULATION

We developed a physics-based simulation environment in MuJoCo [?] and Python, as shown in Fig. ?? (b) and (d), to demonstrate that the behavior of our robot with passive leg stiffness can be modeled with similar approaches using existing tools. For each leg, the four-bar linkage is represented as rigid boxes connected with pin joints; the two types of compliance are treated as torsional springs at the knee joint. The dynamics of the entire servo including its motor, gearbox, and internal position PID controller are modelled as an inertia-spring-damper system, which takes a desired angle as the input and outputs a torque. A maximum output torque constraint and static friction within the motor are also added. This servo model can be implemented by combining a position actuator with a position feedback gain and a force range and a hinge joint with some armature, damping, and friction loss in MuJoCo. Additional boxes are added to match the mass and inertia of various parts of the robot. MuJoCo's default contact model is used for the simulation. The CPG is also implemented in simulation to control the virtual robot.

V. EXPERIMENTS

To validate that our platform is suitable for studying passive leg stiffness in quadrupedal locomotion, we carried out a suite of experiments to evaluate the tunability of the passive leg stiffness, its effect on the robot's performance under two gaits (pronking and trotting), and the feasibility of a simulation environment. Additionally, a video of the robot following remote control command to cruise around is included in the supplemental video.

A. Stiffness Tunability

We designed three variants of the leg, as shown in Fig. ??; leg S1 uses a baseline shape and dimension; for leg S2, the width of both the series and parallel springs are reduced by half; in leg S3 the parallel spring is completely removed and the thickness of the series spring is the same as the rest of the laminate's.

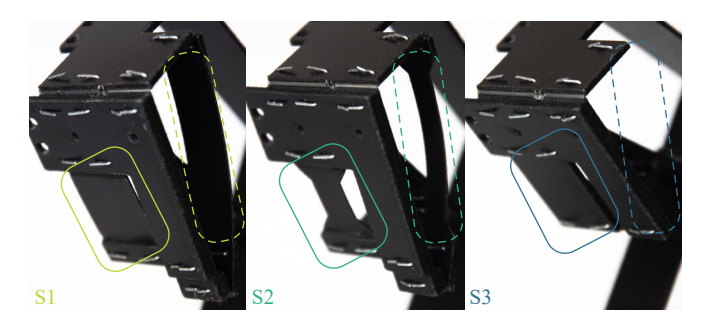


Fig. 5. Pictures of the spring sections of the three leg variants. The flexible links of the series and parallel springs are circled with solid and dashed boxes respectively. The S1 leg has thin, full-width flexible links. The S2 leg has thin, half-width flexible links. The S3 leg has a full-thickness, full-width flexible link in the series spring while the parallel spring is removed.

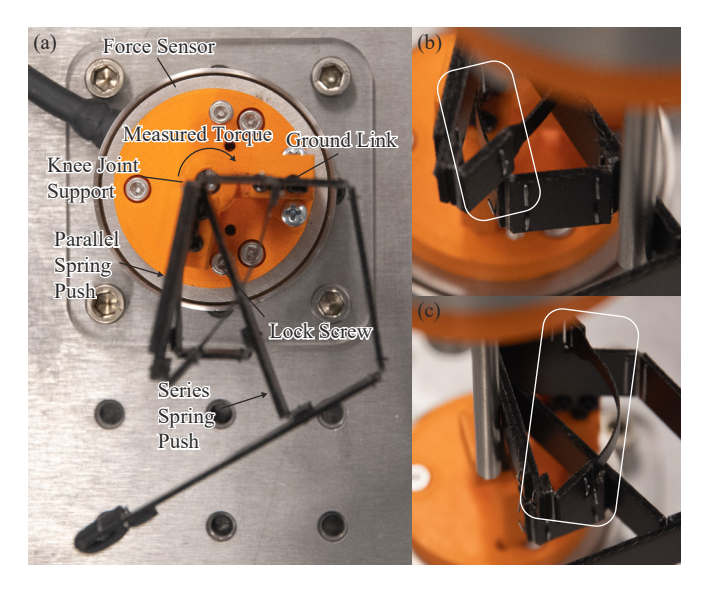


Fig. 6. (a) Experimental setup for measuring the series and parallel stiffness of the leg. (b) Robot pushing the series spring. (c) Robot pushing the parallel spring.

Four samples were fabricated of each leg variant. For each sample, its torque-deformation curve is measured using a static loading setup as shown in Fig. ??. The leg is attached to a force sensor⁶ with a 3D printed jig that only allows knee rotation of the leg. To measure parallel stiffness, the leg's input link is pushed by a robot arm⁷ around the knee joint to only deform the parallel spring. To measure series stiffness, the input link is locked with a screw and the robot arm pushes the crank of the four-bar linkage to deform only the series spring. For both procedures, the robot is commanded to step 0.01 rad every 1.5 seconds until a maximum deformation range is reached, which is conservatively chosen to avoid damaging the leg or sensor. For each step, only the settled section of the force readings are used. The starting point of the spring's deformation is where the torque first exceeds 0.005 Nm. Three trials are performed for each sample and the data are interpolated and averaged to get the stiffness

TABLE I CPG Parameter Values for Experiments

Parameter	Value	Unit	Parameter	Value	Unit
Pronking					
f	$\{1, 2, 3, 4\}$	Hz	$o^h_{FL,FR}$	0.1	rad
d	0.3		$o^h_{RL,RR}$	-0.1	rad
o_r	0		$a_{FL,FR,RL,RR}^k$	1.5	rad
$a_{FL,FR,RL,RR}^{h}$	0	rad	$o_{FL,FR,RL,RR}^{k}$	-0.5	rad
Trotting					
f	$\{1, 2, 3, 4\}$	Hz	$o_{r,f=4,S1,S2,S3}$	0	
d	0.6		$a_{FL,FR,RL,RR}^{h}$	0.5	rad
$o_{r,f=1,S1,S2,S3}$	0.6		$o^h_{FL,FR}$	0.1	rad
$o_{r,f=2,S1}$	0.5		$o^h_{RL,RR}$	-0.1	rad
$o_{r,f=2,S2,S3}$	0.7		$a_{FL,FR,RL,RR}^k$	1	rad
$o_{r,f=3,S1,S2}$	0		$o_{FL,FR,RL,RR}^{k}$	0	rad
$o_{r,f=3,S3}$	0.5				

curve.

B. Pronking

A pronking (jumping with all legs at the same time) experiment was carried out to verify the impact of tuning leg stiffness. For each leg variant, all four samples are first attached to the robot and all servo angles are calibrated to make sure the robot's home pose stays the same. Then, the robot is commanded to pronk in place from rest at various frequencies with the CPG parameter values listed in Table ?? on a level, flat, hard, metal surface. An example of a pronking cycle is shown in Fig. ?? (a). The duration of each run is 20 s, 10 s, 6.67 s, and 5 s for 1 Hz, 2 Hz, 3 Hz and 4 Hz, respectively, so that the number of gait cycles are roughly the same. A USB cable is attached to the rear of the robot for data collection but is kept slack for the entire process. Three trials are carried out per frequency per leg variant. A motion capture system⁸ is used to record the robot's body pose data at 100 Hz.

C. Trotting

A series of trotting runs was also performed to confirm that tuning the robot's leg stiffness affects its running performance. For each leg variant, after the setup procedure similar to the pronking experiment, the robot is commanded to trot forward from standing still at various frequencies with the CPG parameter values listed in Table ?? on a level, flat, hard, and slightly textured surface. At each frequency, most parameters are kept the same except the retraction offset timing o_r whose value requires adjustment to stabilize the gait. An example trotting cycle is shown in Fig. ?? (c). The duration of each run and number of trials follow the pronking experiment. Since the motion capture area is not big enough, a tape measure is used to determine the

⁶ATI Industrial Automation Mini40 IP65/IP68

⁷Universal Robots UR5e

⁸NaturalPoint OptiTrack Prime 17W

distance between the robot's starting and ending positions, which is then divided by the duration of the run to get the average speed. The current through each servo is also recorded at 100 Hz. Given that the supplied voltage is 5V, the average power consumption P can be derived and the cost of transport (COT) computed as $COT = \frac{P}{mgv}$ where $m = 0.396 \, kg$, $g = 9.81 \, m/s^2$, and v is the average speed.

D. Simulation

We performed the same pronking and trotting experiments in simulation and recorded the same performance metrics. Only one trial per frequency was carried out because the model is deterministic. The power term used in the COT calculation is the average positive mechanical power output by all the servos; this is different from the experiment because the electrical power consumption was not computed in simulation.

All the parameter values for the servos are identified by matching the frequency response of a separate MuJoCo model to a set of experiments that swing the servos with increasing frequency with various loads. The friction coefficient is set to 0.39 for both gaits. This value was determined by dragging the robot with a force gauge on the experimental surfaces. Since the damping properties of the leg's springs are unknown, a differential evolution [?] minimization routine using Python's SciPy package was selected to minimize the percentage error of the average velocity and peak height between simulation and experimentation, in order to determine the proper damping coefficients for each leg variant.

VI. RESULTS AND DISCUSSIONS

A. Stiffness Tunability

The measured series and parallel stiffness profiles of all the leg variants are plotted in Fig. ?? and Fig. ??; these figures highlight how series and parallel compliance can be easily tuned in our leg design. The data across different fabricated samples of the same variant also show consistent mechanical properties with low variation. The series spring exhibits nearly linear stiffness, which was expected since it follows our previous design, where linearity was controlled via geometry. On the other hand, the parallel spring, which is new to this work, shows initially stiffer behavior at smaller deflections. Whether this nonlinearity is desirable or not for quadrupedal locomotion remains an open and interesting research question. Counterintuitively, the S3 leg's stiffness profile is relatively similar to the other two, even though it has no intentionally flexible sections. Further investigation indicates that the measured series stiffness is inherent in the structure due to the relatively thin laminates used, while the parallel stiffness measured can be attributed to the stiffness of the mechanisms' flexure joints.

B. Pronking

The average peak body height of the pronking experiment is plotted in Fig. ??. The power of the robot's servos isn't enough to produce a significant height increase. At 1 Hz, the feet of the robot do not leave the ground, and the peak

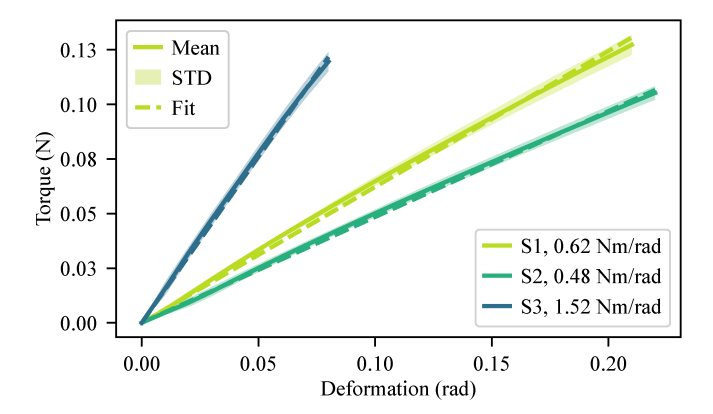


Fig. 7. Series stiffness profiles of the legs.

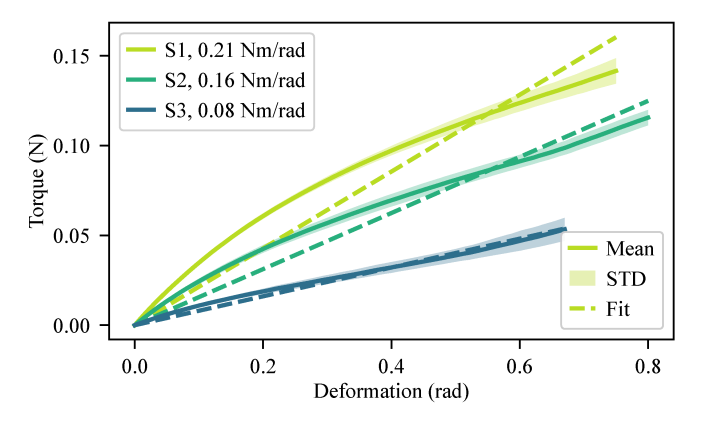


Fig. 8. Parallel stiffness profiles of the legs.

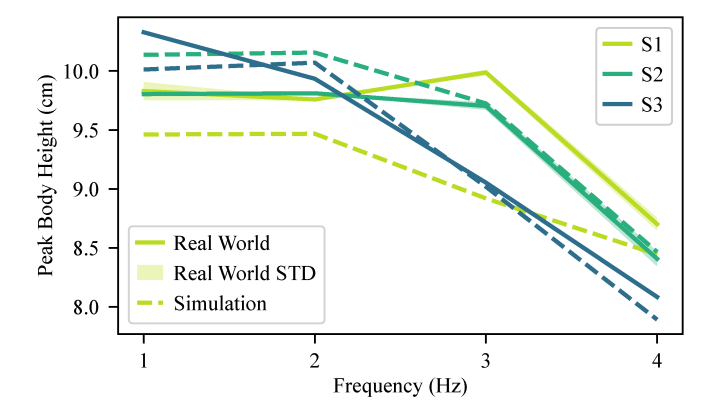


Fig. 9. Average peak body height of the robot pronking with different leg variants at different frequencies.

body height equals the standing height. It should be noted that the robot's standing height is slightly different for each leg variant due to varying leg stiffness. For most cases, the servos can't keep up with the increasing frequency and the actual knee output amplitude drops, resulting in a height loss. However, the stiffness of the S1 leg manages to resonate at the 3 Hz frequency, achieving a small but noticeable height gain. This demonstrates how tuning leg stiffness can achieve better pronking performance.

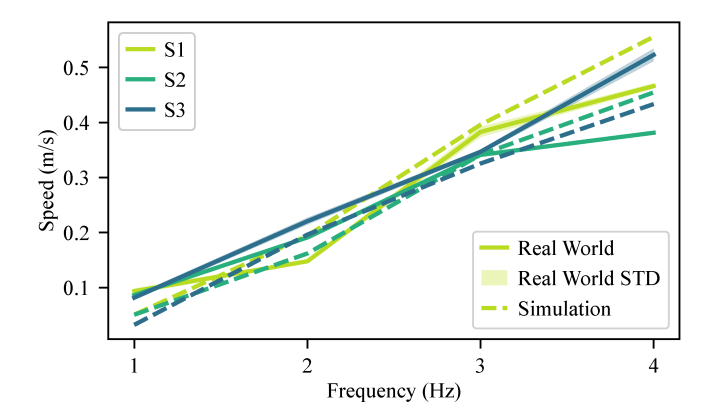


Fig. 10. Average speed of the robot trotting with different leg variants at different frequencies.

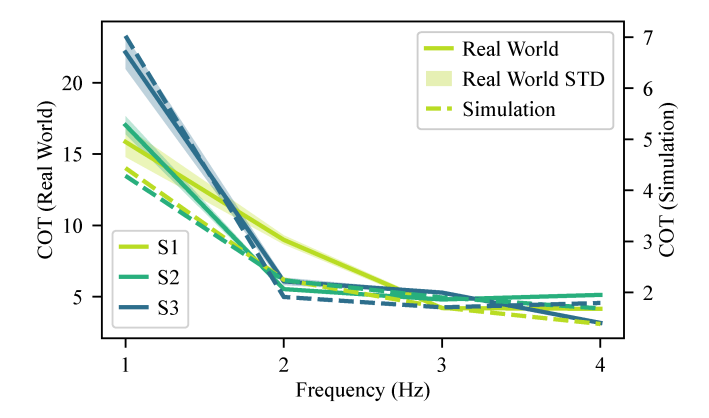


Fig. 11. COT of the robot trotting with different leg variants at different frequencies. The COT has different scales between the real world and simulation results because it uses different power terms as mentioned in section ??.

C. Trotting

The average speed and COT of the trotting experiment are plotted in Fig. ?? and Fig. ??. A nearly linear increase in speed is observed; this is expected since the amplitude of the leg's swing is equivalent across all frequencies while the flight phase remains short. A maximum speed around 0.52 m/s is achieved, equivalent to 4.4 body lengths per second, where a body length is the distance between the front and rear hip joints of the robot. The smallest measured COT was 3.2. At 4 Hz, the best-performing leg design S3 is 37.1% faster in speed and 62.0% more efficient in COT than the worst leg design S2. Interestingly, the best performing leg in terms of speed or efficiency changes as a function of frequency, confirming how optimum passive leg stiffness varies for quadruped robots intended to trot at different frequencies or speeds.

D. Simulation

The simulation results are plotted alongside the real-world results in Fig. ??, Fig. ??, and Fig. ?? and the average percentage error of the average trotting speed and pronking peak height is 12.7%. The general trends of the pronking and trotting performance match well but the best performing legs

at some frequencies differ from the real-world experiments; this is probably due to the inaccuracy of the contact model, the absence of the cable-driven mechanism model, and the "parasitic" compliance of the supposedly rigid laminate links. There are several potential options for narrowing this sim-to-real gap: remove the cable-driven mechanism and switch to a simpler serial actuation scheme, increase the thickness of the leg links to improve rigidity, and perform more comprehensive characterization experiments. With further tweaking and calibration, the simulation environment is expected to represent the robot better and contribute to future study.

VII. CONCLUSIONS

The design of a quadruped robot with compliant laminate legs has been presented in detail, along with initial results that demonstrate the potential for varying passive leg stiffness for tuning pronking and trotting performance. Future work will continue to improve the robot's design and control while maintaining a focus on affordable and accessible approaches. Ways to widen the range of the leg stiffness and tune other properties such as damping and leg travel length will be explored. Studies of the robot's ground reaction force generation capability and its relationship with the leg stiffness will be performed to better understand and estimate its locomotion capabilities. The accuracy of the simulation environment will be improved and design space constraints of the legs will also be included for optimization and learning purposes. Using this platform, we envision exploring many potential research questions, such as how to develop model-based control or learning algorithms that can identify and better exploit variable, passive leg stiffness than the CPG used in this paper, the role of parallel and series compliance in tuning different gaits across various locomotion metrics, and whether the proposed design can be scaled up and applied to existing commercially available legged robots. We believe this platform has the potential to increase accessibility to legged robotic locomotion, with potential applications in education, agriculture, and other applications in which tunability, simplicity, and affordability remain constraints.

ACKNOWLEDGMENT

This material is based upon work supported by the National Science Foundation under Grant No. 1944789.